ADVANCES IN ATMOSPHERIC SCIENCES, VOL. 30, NO. 3, 2013, 607–620

Performance of FGOALS-s2 in Simulating Intraseasonal Oscillation over the South Asian Monsoon Region

HU Wenting (胡文婷), DUAN Anmin* (段安民), and WU Guoxiong (吴国雄)

State Key Laboratory of Numerical Modeling for Atmospheric Sciences and Geophysical Fluid Dynamics, Institute of Atmospheric Physics, Chinese Academy of Sciences, Beijing 100029

(Received 5 July 2012; revised 15 November 2012)

ABSTRACT

The capability of the current version of the air-sea coupled climate model, the Flexible Global Ocean-Atmosphere-Land System model, Spectral Version 2 (FGOALS-s2), in simulating the boreal summer intraseasonal oscillation (ISO) over the south Asian monsoon (SAM) region is diagnosed, in terms of dominant period, propagation direction, and vertical structure. Results show that the coupled model can reasonably simulate the main features of observed ISO propagation compared to the chosen AGCM. These features include the eastward movement of intraseasonal 850-hPa zonal wind over the Arabian Sea and Bay of Bengal, the vertical structure in active phases, and the realistic phase relationship between ISO and underlying SST. However, the eastward propagation cannot be reproduced in the uncoupled model. This suggests that air-sea interaction is important in generating intraseasonal variability over the SAM region. Nevertheless, some deficiencies remain in the coupled model, which may relate to physical processes depicted by the cumulus parameterization and PBL schemes within its atmospheric component.

Key words: intraseasonal oscillation, numerical simulation, eastward propagation, air-sea interaction

Citation: Hu, W. T., A. M. Duan, and G. X. Wu, 2013: Performance of FGOALS-s2 in simulating intraseasonal oscillation over the South Asian monsoon region. *Adv. Atmos. Sci.*, **30**(3), 607–620, doi: 10.1007/s00376-013-2156-6.

1. Introduction

The tropical intraseasonal oscillation (ISO) has great impacts on the characteristics and evolution of the Asian summer monsoon, especially its onset and break (e.g. Yasunari, 1979, 1980; Lau and Chan, 1986; Nakazawa, 1992; Wang and Xu, 1997; Wu and Zhang, 1998; Kang et al., 1999; Kemball-Cook and Wang, 2001; Waliser et al., 2003). Since ISO is considered to result from the interaction between tropical convection and large-scale circulation (e.g. Seo and Wang, 2010), its prediction can fill the gap between weather forecasting and climate prediction (e.g. Hendon et al., 2000; Yang et al., 2009). Therefore, evaluation of general circulation model (GCM) ISO is necessary for improving simulations and predictions of the Asian summer monsoon.

Although most GCMs have improved in simulating general atmospheric behavior in recent years, the simulation of the Madden Julian Oscillation (MJO) is still model-dependent and its attainment has been limited (e.g. Waliser et al., 1999; Hendon et al., 2000; Inness and Slingo, 2003; Fu et al., 2008; Kim et al., 2009). Simulation of the boreal summer ISO over the south Asian monsoon (SAM) region has received much attention, but major challenges remain. Intraseasonal variability of the SAM is difficult to reproduce in GCMs, because it is influenced by unique underlying surface conditions, mean flow and vertical structure, compared to equatorial areas (e.g. Annamalai and Slingo, 2001; Teng and Wang, 2003; Jiang et al., 2004; Liu et al., 2007). Based on 10-member ensembles of two-year simulations from 10 different AGCMs, Waliser et al. (2003) demonstrated that ISO patterns in most models exhibited some form of northeastward propagation. However, the patterns lacked coherency, adequate eastward propagation, and were on spatial scales that were too small.

As the effects of oceans were introduced into climate models, interest grew about the effects of air-

*Corresponding author: DUAN Anmin, amduan@lasg.iap.ac.cn

sea interactions on ISO simulations (e.g. Fu et al., 2002; Fu and Wang, 2004; Zhang et al., 2006; Fu et al., 2007). Zhang et al. (2006) assessed four pairs of coupled and uncoupled simulations to demonstrate that air-sea coupling indeed strengthens the eastward-propagating signal of the MJO, but it has inconsistent effects on phase relationship, coherence, geographic distribution, seasonal cycles and interannual variability. Fu and Wang (2004) used an atmosphere-ocean coupled model and an atmosphere-only model. They found that the coupled model produced a more realistic ISO, because it simulated high coherence between precipitation and SST. However, certain model biases still exist in coupled models. The diagnostic results of 14 coupled GCMs that participated in the IPCC Fourth Assessment Report (AR4) carried out by Lin et al. (2006), revealed that only two could reproduce the MJO variance and predominant 30–60-day period spectral peak compared to observations. This failure to simulate the realistic MJO is presumed to relate to uncertainties of interactions between physical parameterization schemes, and to deficiencies in capturing multiscal'e interaction (e.g. Chao and Deng, 1998; Lee et al., 2003; Liu et al., 2005; Wang, 2005). Lin et al. (2008a) evaluated intraseasonal variability associated with the Asian summer monsoon in 14 coupled GCMs. They found that although the models simulate the northward ISO propagation well, they often have difficulty in simulating its eastward movement.

The off-equatorial eastward movement of convection, which is a robust feature of the summer ISO, has not received enough attention (Lawrence and Webster, 2002). Thus, we evaluate the simulations of eastward-propagating ISO over the SAM region in both the current version of the air-sea coupled climate model, the Flexible Global Ocean-Atmosphere-Land System model, Spectral Version 2 (FGOALS-s2), and its atmospheric component, the Spectral Atmospheric Model of IAP LASG (SAMIL 2.4.7).

The paper is organized as follows. Section 2 describes the observational datasets, model and statistical methods. In section 3, simulation results are presented, in order to show the differences between SAMIL2.4.7 and FGOALS-s2. The potential contributions from air–sea interaction are described in section 4. Finally, a discussion and conclusions are given in section 5.

2. Data, model and methods

2.1 *Datasets*

To evaluate the capability of FGOALS-s2, the observational datasets used here are as follows: (1) National Centers for Environmental Prediction (NCEP) Reanalysis 2 (NRA-2) (NCEP-R2), from 1979 to 2005 with 2.5°×2.5° spatial resolution. Wind fields and other 3D variables, including vertical velocity and specific humidity, are derived from the NCEP-R2 dataset. (2) National Oceanic and Atmospheric Administration (NOAA) interpolated outgoing longwave radiation (OLR; Liebmann and Smith, 1996), from 1979 to 2005 with 2.5°×2.5° spatial resolution, which can be considered as a reasonable substitute for precipitation in the tropics. (3) The precipitation dataset from the Global Precipitation Climatology Project from 1979 to 2005 (GPCP; Huffman et al., 1997; Adler et al., 2003). (4) NOAA Optimum Interpolation (OI) SST V2 (OISST; Reynolds et al., 2002) daily mean data with 1°×1° spatial resolution, from 1990 to 2004. (5) Daily mean net surface full-sky shortwave radiation flux derived from the International Satellite Cloud Climatology Project (ISCCP) (Schiffer and Rossow, 1985) with 1°×1° spatial resolution, from 1990 to 2004. (6) Daily mean surface latent heat flux derived from the Objectively Analyzed air–sea Heat Fluxes (OAFlux) project (Yu et al., 2008) with 1°×1° spatial resolution, from 1990 to 2004.

2.2 *Model and experimental description*

FGOALS-s2 contains five active components, detailed descriptions of which can be found in Bao et al., 2010. The atmospheric component is version 2.4.7 of SAMIL. In the horizon, SAMIL2.4.7 is rhomboidally truncated at a zonal wave number (R42), roughly equal to a grid of 2.8125° (lon)×1.66° (lat). It has 26 atmospheric layers, from the surface to a top at 2.5 hPa. The radiation scheme is from Edwards and Slingo (1996), modified by Sun and Rikus (1999a, b). Cumulus parameterization uses the Tiedtke scheme (Nordeng, 1994; Song, 2005). The oceanic part is the LASG IAP Climate Ocean Model (LICOM) (Liu et al., 2004), with higher resolution (0.5°×0.5°) in the tropics. The PBL scheme was developed by Brinkop and Roeckner, 1995 to calculate the turbulent transfer of momentum, heat, moisture, and cloud water.

Following the request of the IPCC Fifth Assessment Report (AR5), two kinds of experiments were conducted, which were AMIP (Atmospheric Model Intercomparison Project) and CMIP (Coupled Model Intercomparison Project) (Taylor et al., 2009). In the AMIP run, observed SST and sea ice temperature from 1979 to 2008 were used as boundary forcing data, and realistic greenhouse gas, solar constant and aerosol were specified. The CMIP run was integrated from 1850 to 2005. To improve comparison with observational data, the same 27-yr period (1979–2005) was chosen for both AMIP and CMIP simulations.

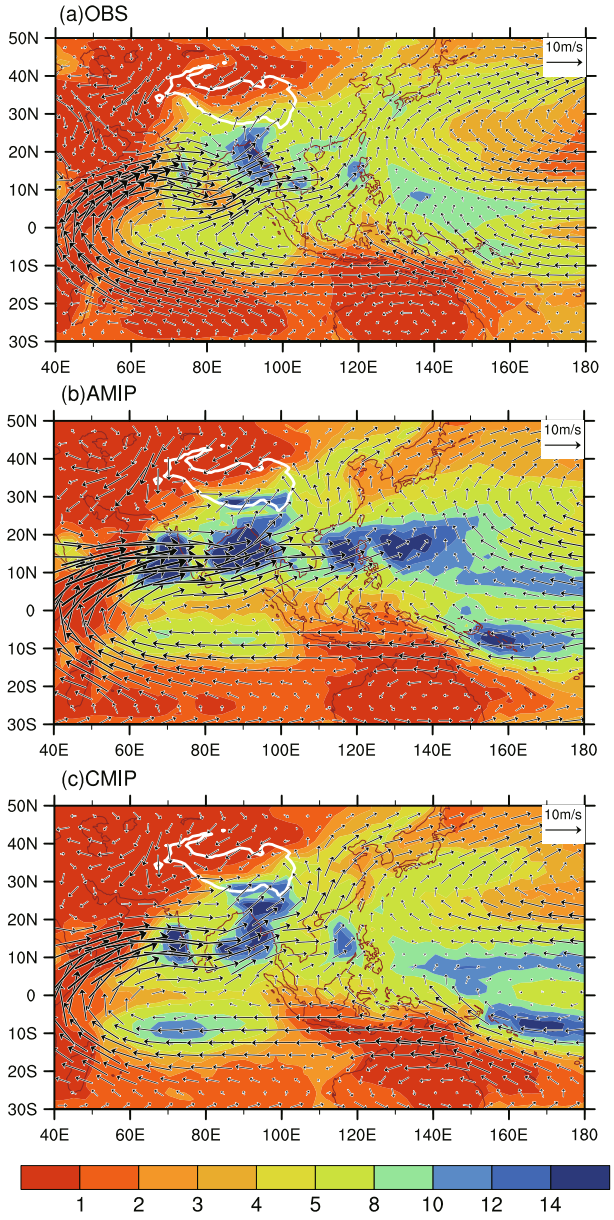

Fig. 1. Summer mean (JJA) precipitation (shading; mm d^{-1}) and 850-hPa wind fields (vectors; m s^{-1}) for the 27-yr period 1979–2005: (a) observations; (b) AMIP; (c) CMIP.

2.3 *Statistical method*

Since the intraseasonal variability of the monsoon is active in boreal summer, we selected 27 summer half-years (May–October) from 1979 to 2005, to analyze ISO characteristics and evolution. Before other calculations, the annual cycle and temporal mean were removed from both model outputs and observational data to obtain the anomalies. Wavenumber-frequency diagrams can represent the predominant spatial and temporal scales of ISO over the SAM region. In this study, the anomalies were bandpass-filtered to isolate the ISO signal.

Composite analysis and the Student's t-test are used to demonstrate the life cycle of boreal summer ISO. Each t-score of related variables was calculated; when it is larger than the t-value at 95% in the Student's t distribution, the null hypothesis of no relationship is rejected. Only results passing the t-test are plotted in the composite figures.

3. Simulation results

3.1 *ISO predominant period*

Realistic reproduction of the climate mean pattern, in both general circulation and precipitation, is a precondition for successful simulation of intrasea sonal variability (Wheeler and Kiladis, 1999). First, we examined the performance of the climatological mean monsoon simulations in boreal summer. Figure 1 shows observed and simulated June–August mean precipitation and 850-hPa wind fields. Both models capture the features of the cross-equatorial Somali jet and strong westerlies over the SAM region in the lower troposphere. The gross pattern of summer mean precipitation, such as the rainfall centers over the Bay of Bengal (BOB) and Philippines are reproduced by the models, although the amount of rainfall is overestimated. Compared to the AMIP run, the rainfall amount of the CMIP run over the SAM region and Western Pacific is more realistic, but still larger than the observations. This may be directly related to imperfect physical processes in the model, particularly the cumulus convective parameterization scheme.

Many studies have used wavenumber-frequency spectral analysis to investigate the spatial and temporal scales of tropical convection, for zonally-propagating waves (Hayashi, 1982) and meridionally-propagating disturbances in the Indian Ocean area (Fu and Wang, 2004). Figure 2 shows wavenumber-frequency spectral diagrams of 850-hPa zonal wind for 27 summer half-years, averaged over the 10°–20°N latitude band, from the reanalysis and models. In the reanalysis (Fig. 2a), the low-frequency eastward variance in boreal summer, which of maximum value is 0.08 m^2 s^{-2} clearly dominates the westward counterparts. The predominant period is 40–80 days, which is considered a basis for isolating ISO signals in the following analysis. Results of the AMIP and CMIP runs are given in Figs. 2b and c. The mainly eastward-propagating disturbances with lower frequencies (greater than 80 days) are commensurate with westward disturbances in the two models. Nonetheless, the magnitude during the 40–80-day period simulated by FGOALS-s2 is closer to the reanaly-

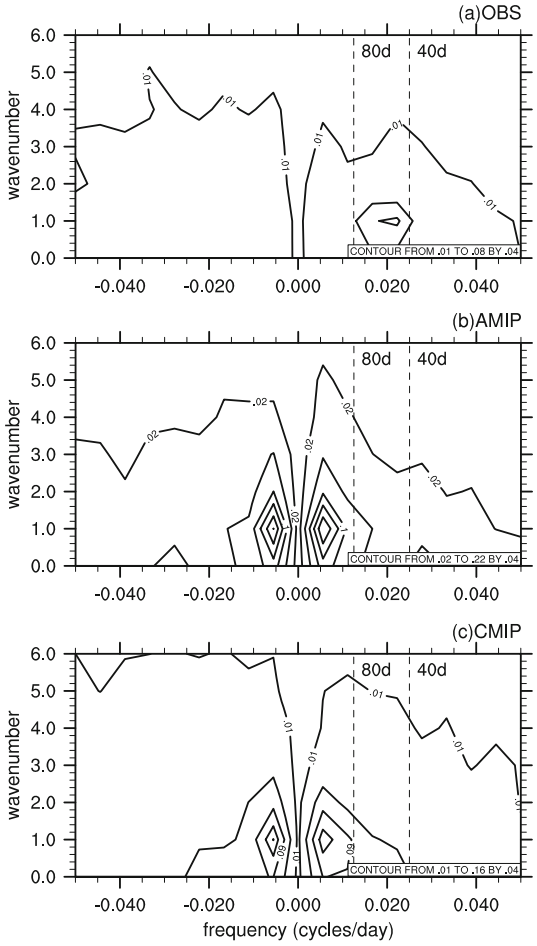

Fig. 2. May–October wavenumber-frequency spectra of 10°–20°N-averaged 850-hPa zonal wind anomalies for the 27-yr period 1979–2005: (a) observation; (b) AMIP; (c) CMIP. Units are m^2 s^{-2} per frequency interval per wave number interval.

sis than in AMIP.

Figure 3 shows the horizontal distribution of explained variance in percentage of intraseasonal variability (40–80-day filtered 850-hPa zonal wind anomaly) during northern summer (May–October). It aims to detect the spatial distribution of intraseasonal variance, in addition to examining the spectra in the global view through the wavenumber-frequency spectral methodology. The observed intraseasonal variability percentage has a maximum over the South China Sea (SCS), which exceeds 13% (Fig. 3a). The center of variance was captured in CMIP with similar amplitude to that observed in the SCS region (Fig. 3c). However, the variance in percentage of 40–80-day filtered zonal wind anomaly simulated by AMIP (Fig. 3b) shows smaller amplitude of center over the SCS and other centers in other regions (the near-equatorial Indian Ocean and the northern Pacific).

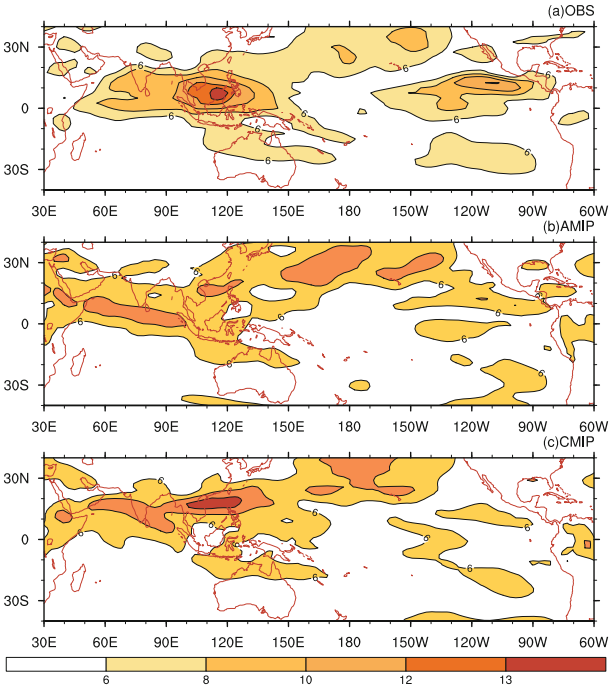

Fig. 3. Horizontal distribution of explained variance in percentage of 40–80-day filtered 850-hPa zonal wind anomaly in boreal summer (May–October): (a) observation; (b) AMIP; (c) CMIP.

To demonstrate the propagation and time-varying features of the ISO over the SAM region, lag-longitude and lag-latitude correlation analyses were also executed. Figure 4 shows the lag-longitude and lag-latitude diagrams of intraseasonal OLR anomalies (colors) and 850-hPa zonal wind anomalies (contours), correlated with area-averaged OLR (10°–20°N, 80°–110°E) during boreal summer. The principal observed characteristics of the 40–80-day filtered ISO are as follows: convection propagates eastward from 40°E to 120°E, moves westward to the east of 120°E, and the propagation of 850-hPa zonal wind is consistently eastward from 40°E to 180°E; there is clear northward spread of OLR and 850-hPa zonal wind anomalies from 10°S to 30°N. No matter the type of propagation, OLR leads 850-hPa zonal wind by about five days. Compared with AMIP, the CMIP run clearly reproduces the eastward propagation of 850-hPa zonal wind from 40°E to 120°E, although there is westward propagation to the east of 120°E. This suggests the contribution of air-sea interaction to generating and maintaining ISO in the SAM region.

3.2 *ISO evolution*

The phase compositing method is often used to understand the evolution of ISO over an entire cycle. To better depict the eastward propagation over the SAM

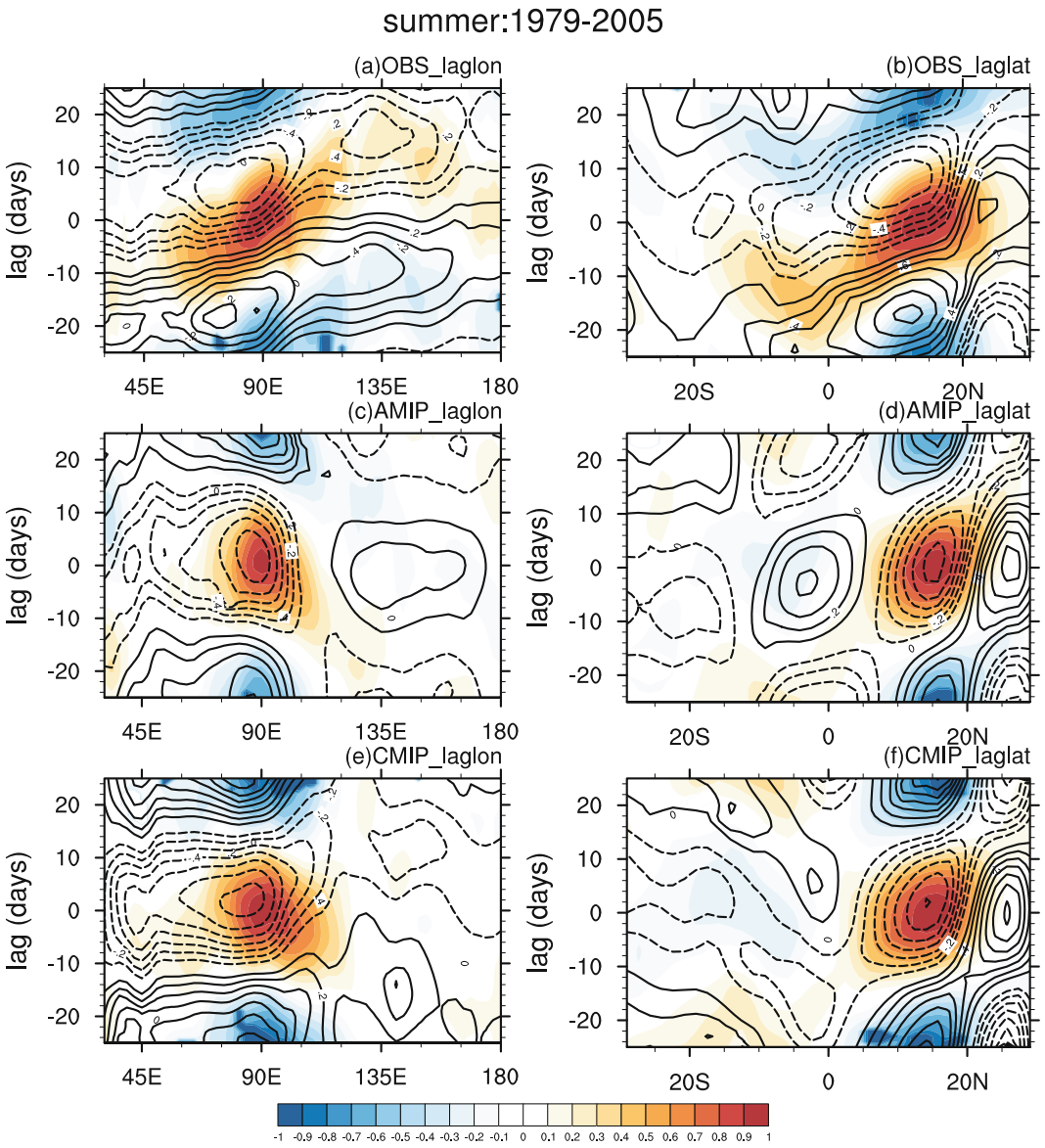

Fig. 4. Summer half-year (May–October; 1979–2005) lag-longitude diagrams of 10°–20°N-averaged, 40–80-day filtered, OLR anomalies (colors) and 850-hPa zonal wind anomalies (contours), correlated with basic area-averaged time series over the Bay of the Bengal: (a) reanalysis; (c) AMIP; (e) CMIP. (b), (d), (f) Observed and simulated lag-latitude sections of 80°–100°E-averaged intraseasonal OLR and 850-hPa zonal wind anomalies, respectively.

region, the 40–80-day filtered and area-averaged OLR anomalies over the BOB (10°–20°N, 80°–100°E) were selected as a basic index for identifying the ISO. As is known, an ISO cycle can be defined as one with a positive and negative anomaly (or an inactive and active period), both of which must have peak amplitudes greater than one standard deviation from zero (Mao and Chan, 2005). Based on this selection criterion, several cycles were determined for the 40–80-day mode from 27 years of data (1979–2005), in both reanalysis and models. Each cycle was divided into nine phases for the compositing analysis. Phase 3 is the peak of the inactive period (OLR anomaly maximizes, corresponding to minimum precipitation over the BOB), and Phase 7 is the peak of the active period (largest rainfall amount over the BOB). Phase 1 is similar to Phase 9, indicating transition from active to inactive periods. Phase 5 is the transition from inactive to active. The times of Phases 2, 4, 6 and 8 are specified when the disturbance reaches half its maximum or minimum value.

Using the compositing technique, evolution of ob-

served intraseasonal 850-hPa winds (vectors) and OLR anomalies (colors) during an ISO cycle is shown in Fig. 5, which indicates significant eastward propagation of 40–80-day ISO over the SAM region. Only OLR anomalies and wind vectors passing the 95% statistical test are plotted. In Phase 1, a positive OLR anomaly center occurs over the northern Arabian Sea, moves eastward and reaches a maximum over the BOB in Phase 3, which corresponds to a conspicuous anticyclone. By Phase 4, the anomalous BOB anticyclone begins to disappear, while deep convection develops along the equator. In Phase 5, the center of this convection moves from the equatorial area to the Arabian Sea, and intensifies in Phase 6. From Phase 7 to 9, the convection moves east and ultimately disappears over the SCS.

The evolution simulated by the AMIP and CMIP runs can be identified in Figs. 6 and 7. Because of the basic index definition, maximum and minimum values occur over the BOB in Phase 3 and Phase 7, respectively. By Phase 8, the ISO signal begins to disappear over the BOB, instead of propagating further east to the SCS. Despite this deficiency, the CMIP run produces a more significant eastward movement of convection and corresponding wind vectors, from the Indian Ocean to BOB (Fig. 7). In the AMIP run, however, simulated ISO propagation is weak (Fig. 6).

To further investigate the vertical structure of eastward-propagating ISO and to explain the failure of the convection center to move into the SCS in the CMIP run, a series of pressure–longitude plots are used to show differences between the model and observations. The diagnosis variables include 2D (pressure and longitude) vorticity, vertical velocity and moisture divergence, with respect to the latitude of the convection center in Phases 7 and 8 (Figs. 8 and 9, respectively). The minimum value of OLR anomalies represents the longitude at the location of the convection center (Fig. 8g, h and Fig. 9g, h). The latitudes of the convection center in Phase 7 and Phase 8 in the observations are 12°N and 10°N respectively, 14°N and 15°N in the CMIP run. The left panels of Figs. 8 and 9 are derived from the CMIP run, and the right panels from the reanalysis.

From the reanalysis in Phase 7, as the rainfall center moved over the BOB (approximately 90°E; Fig. 7h), maximum vertical motion occurred in the mid troposphere (Fig. 8d), and lower-layer moisture convergence (Fig. 8f) with baroclinic vorticity structure (Fig. 8b) coincided with the convection center. To the east of the convection center (over the SCS), a positive vorticity center with equivalent barotropic structure appeared, corresponding to a moisture convergence center in lower layers. In the CMIP run, the structure is very similar to the reanalysis, with comparable magnitude. Over the SCS, the PBL moisture convergence is restrained, corresponding to a lower tropospheric, negative vorticity center that induces downward motion. This may be why the convection could not develop over the SCS, and it implies that PBL physical processes affect the generation of the next convection center.

As a consequence, the simulated convection center with weak upward motion and moisture divergence begins to diminish over the BOB in Phase 8 (Fig. 9). Because of the undeveloped convection over the SCS, the eastward advance of convection is restrained in the simulations. In contrast, the observed vertical structure over the SCS is similar to that over the BOB in Phase 7.

4. Potential contributions of air-sea interaction

The coherent evolution between the atmospheric component and underlying SST or SST tendency associated with ISO is important in the ISO simulations. The effects of air-sea interaction can be evaluated by the lag correlation method (e.g. Fu and Wang, 2004; Wu and Kinter, 2010). Figure 10a presents the observed and simulated relationship between pentad precipitation and SST, and Fig. 10b shows the correlation between rainfall and SST tendency. Lag correlations are calculated by area-averaged (10°–15°N, 112°–117°E) anomalies. The pentad-mean SST tendency uses the method of centered differencing; that is, the SST difference between the next and previous pentads.

Over the SCS, the coupled solution is more consistent with the observations, although the correlation coefficient is smaller. Lacking the influences of air–sea interaction, the AMIP run fails to represent the correct relationships of precipitation and SST/SST tendency. In the coupled case (CMIP), positive (or negative) SST leads (or lags) convection by about 2–3 pentads, with a correlation coefficient of 0.4 (or −0.4). However, in the atmosphere-only run (AMIP), SST is almost in phase with rainfall. In contrast, the relationship between rainfall and SST tendency in the observations is similar to the CMIP run, very different from the uncoupled result. These findings reiterate that the intraseasonal convection in the AMIP run is less coherent with the underlying SST/SST tendency, compared to the CMIP run.

In order to analyze the spatial patterns of surface heat fluxes and moisture convergence during the wet phase and then detect the surface physical processes, Figs. 11–13 were produced to show the differ-

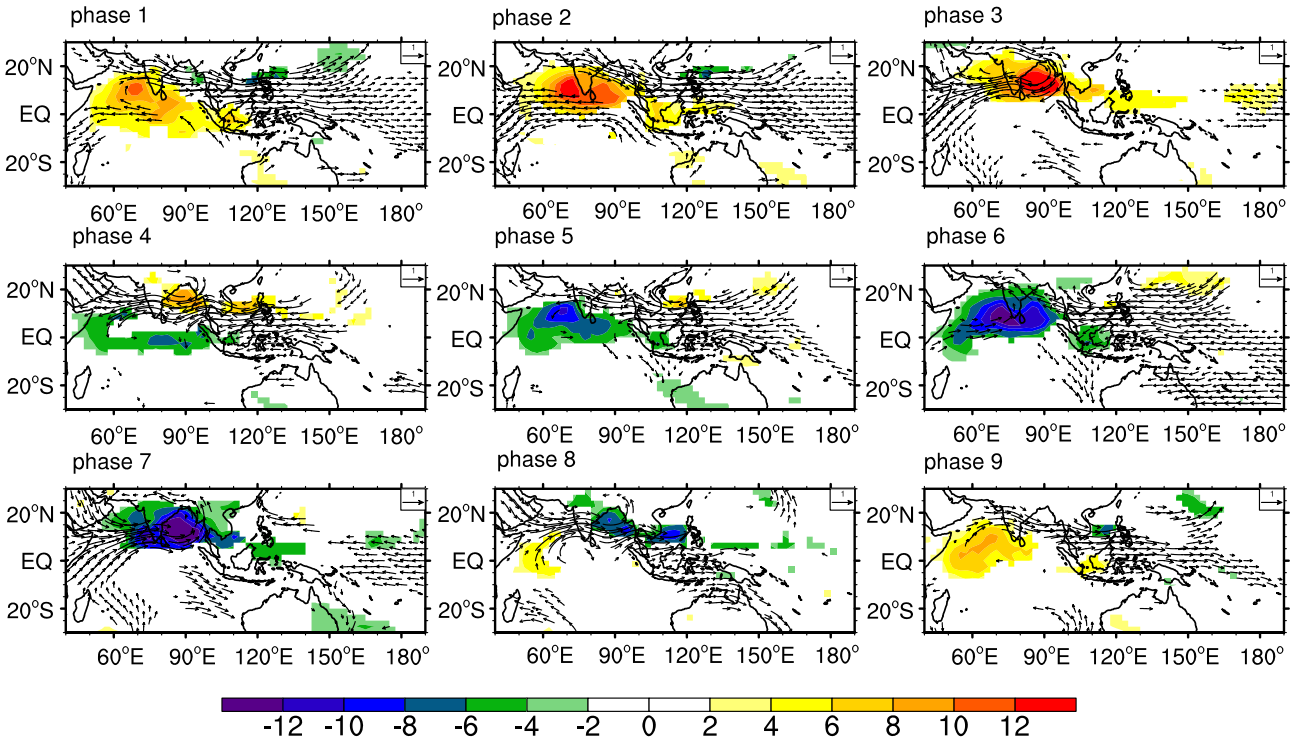

Fig. 5. Composite evolutions of 40–80-day filtered 850-hPa winds (vectors; m s^{-1}) and OLR anomalies (shading; W m^{-2}) during an ISO cycle from reanalysis. Phases 1–9 are displayed. Only significant OLR anomalies and wind vectors are plotted.

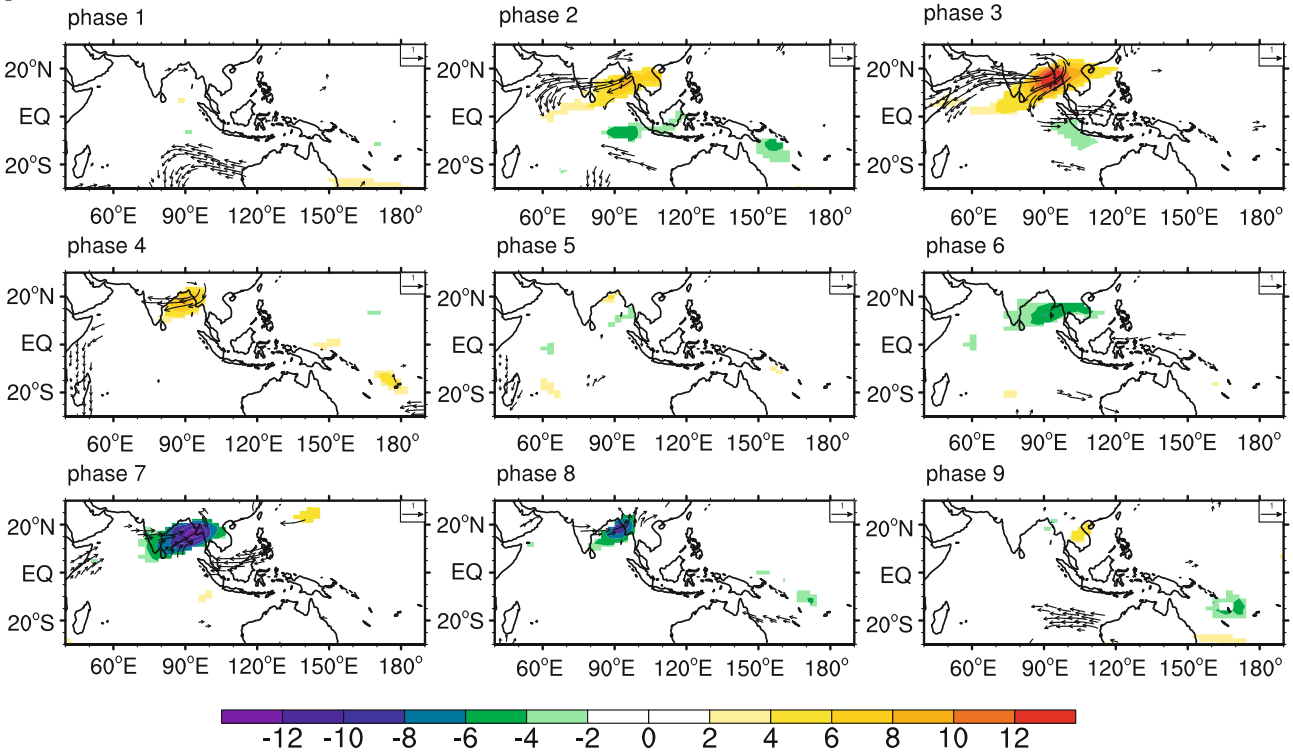

Fig. 6. The same as Fig. 5, but from calculated AMIP data.

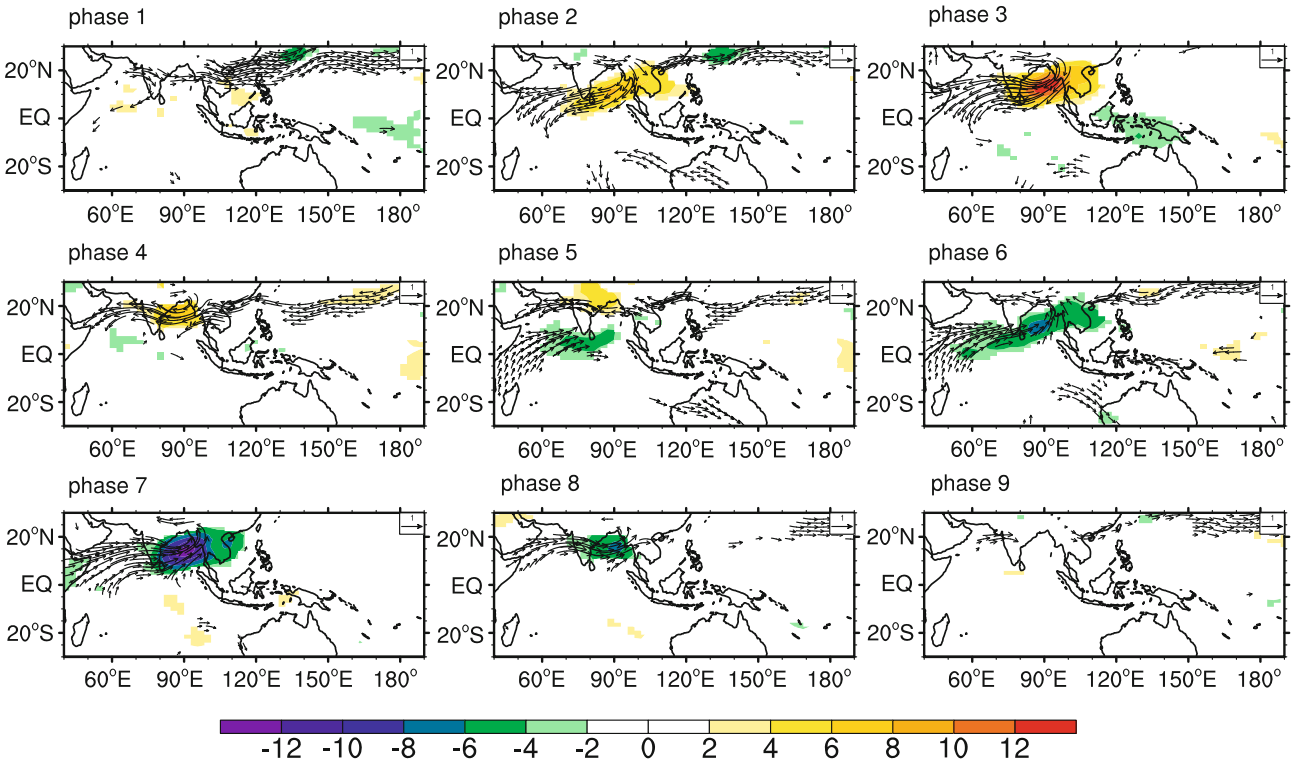

Fig. 7. The same as Fig. 5, but from calculated CMIP data.

ences among the observations, the AMIP and CMIP in Phase 7. In the observations, the net surface heat flux (Fig. 11a) indicates a positive value over the Asian summer monsoon, with two maxima located over the BOB and SCS. The simultaneous upward net surface shortwave radiation flux (Fig. 11b) in the SCS implies the high SST warms the local atmosphere and then moisture convergence occurs (Fig. 11c). The surface fluxes and moisture convergence simulated by CMIP (Fig. 13) are closer to those in the observed than in AMIP (Fig. 12), which demonstrates the SST over the SCS in the coupled model during the wet phase presents warmer and has a better phase relationship with precipitation (Fig. 10). However, it still has some deficiencies; for example, the amplitude of surface fluxes is not large enough to generate strong moisture convergence.

The atmospheric ISO signals can form coherent SST disturbances, which provide a reasonable forcing field. Positive SST influences PBL moisture convergence through upward heat flux east of the convection center, aiding the eastward motion of convection. On the other hand, sea surface cooling prevents the development of convection at its original location. The PBL moisture convergence intensified because of the elimination of this original convection, triggering new convection. In short, air-sea interaction cannot be neglected in the reproduction of realistic intraseasonal variability over the SAM region.

5. Conclusions and discussions

We evaluated the performance of intraseasonal variability over the SAM region in FGOALS-s2 and its atmospheric component SAMIL2.4.7. The main conclusions can be summarized as follows.

The CMIP run of FGOALS-s2 successfully simulated the eastward movement of intraseasonal 850-hPa zonal wind from 40°E to 120°E, and produced a more realistic vertical structure during active phases, as compared to the AMIP run of SAMIL2.4.7. However, there are noteworthy weaknesses in the coupled case. To the east of 120°E, the simulated intraseasonal 850-hPa zonal wind moved westward.

Furthermore, composite analysis indicated that the eastward propagation simulated by the CMIP run is more obvious than the AMIP run, but deficiencies still exist. The most notable failure is that the ISO signals ultimately begin to disappear over the BOB, instead of propagating eastward to the SCS. The possible cause may be weak vertical motion and a near-surface negative vorticity center over the SCS during the active phase.

The greatest difference between the AMIP and

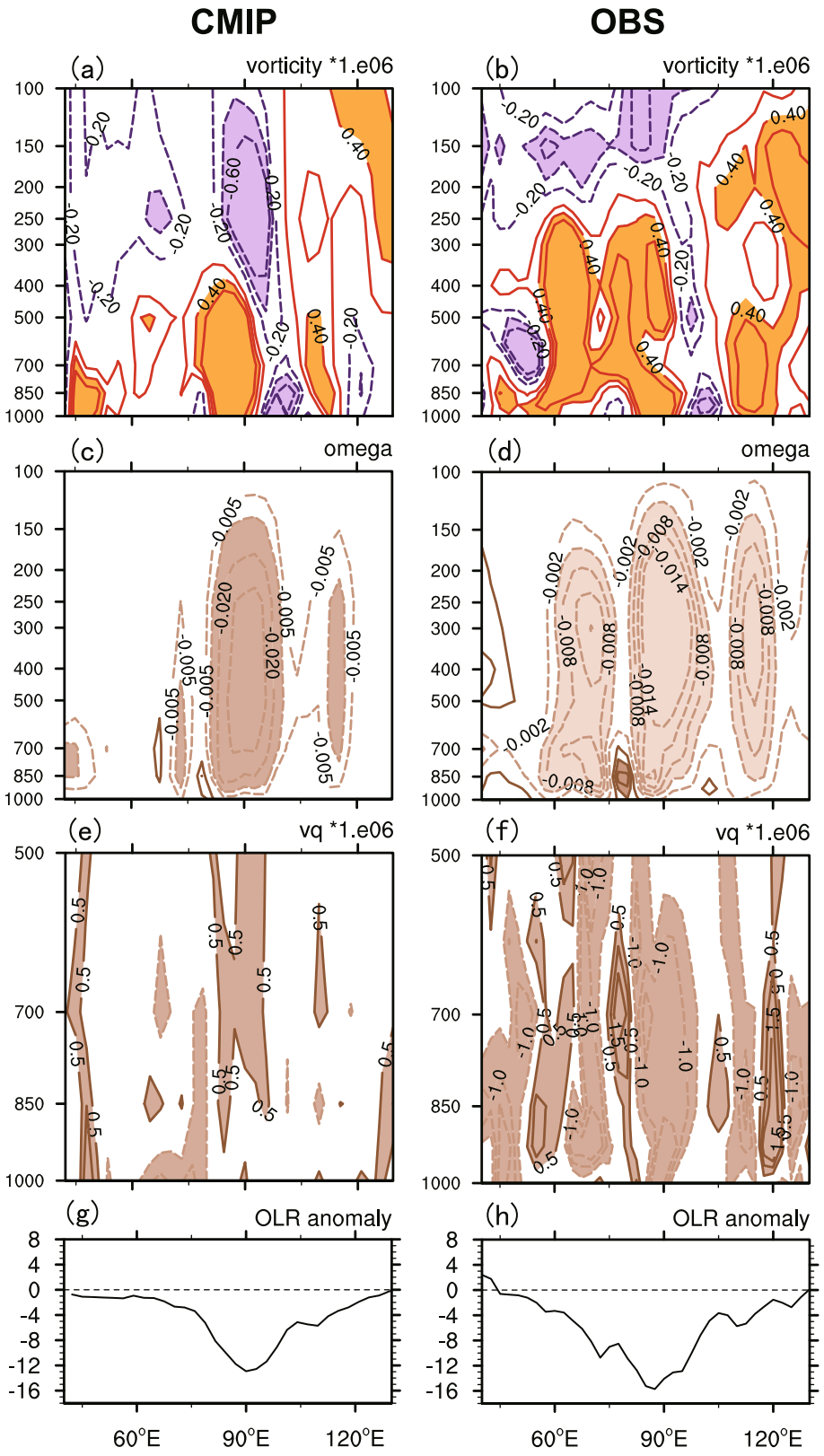

Fig. 8. Pressure-longitude cross sections of vorticity (10^6 s^{-1}), vertical velocity (Pa s^{-1}), moisture divergence (10^6 g kg^{-1} s^{-1}) and amplitudes of OLR anomalies (W m^{-2}) during Phase 7 from CMIP data (left panel) and reanalysis data (right panel), with respect to latitude of convection center.

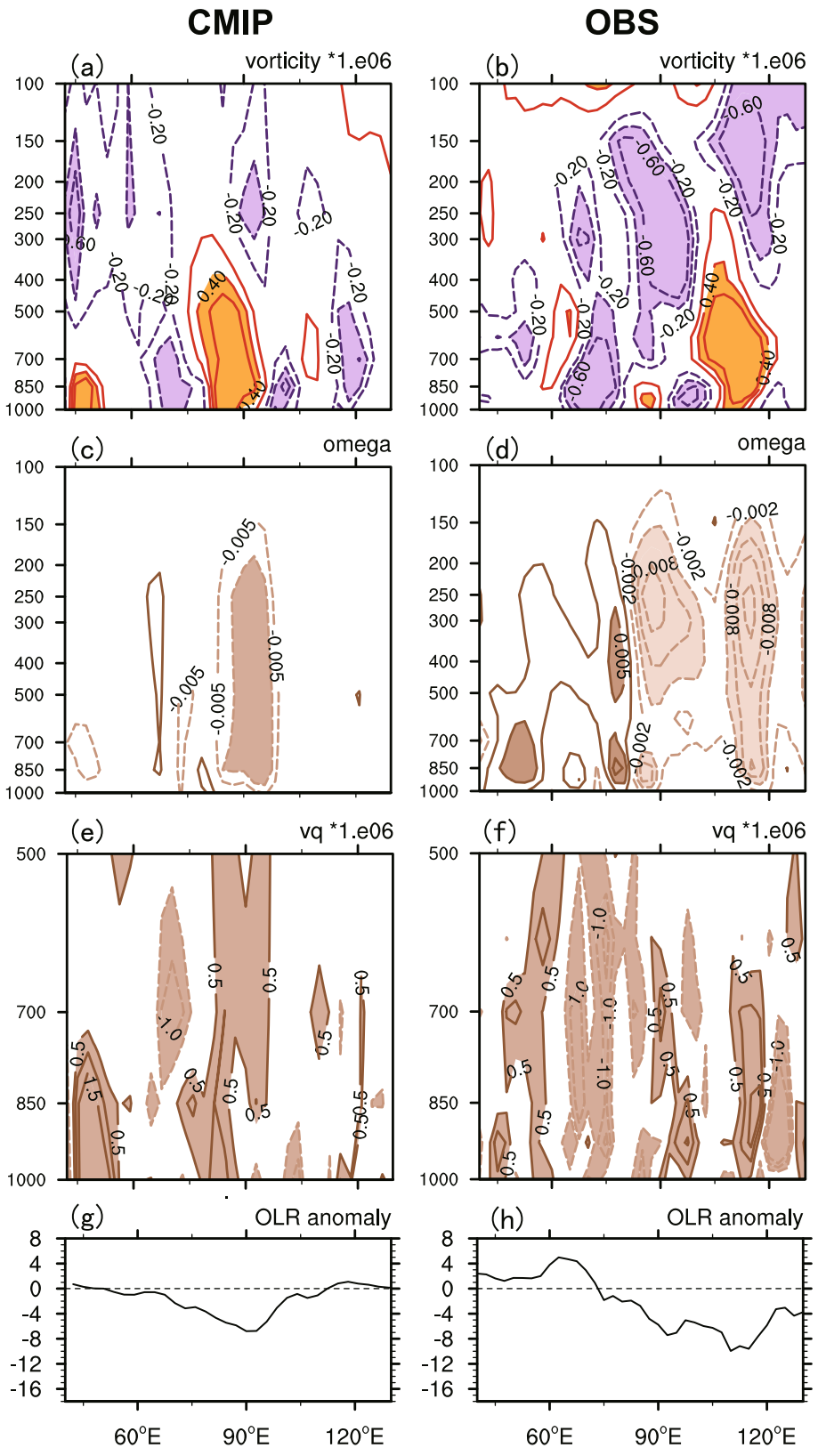

Fig. 9. The same as Fig. 8, but for Phase 8.

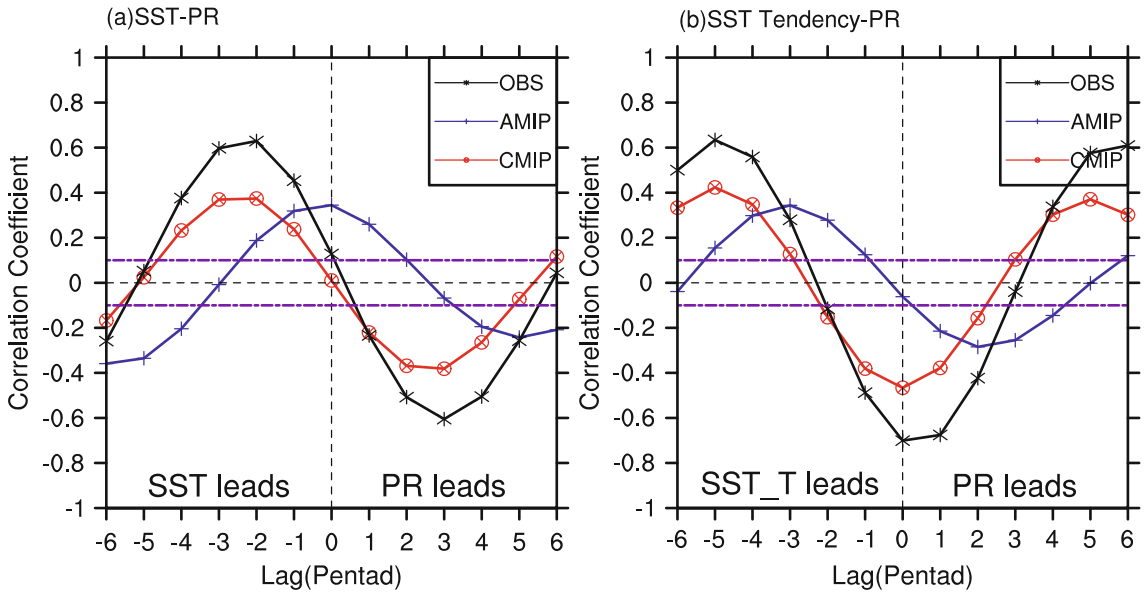

Fig. 10. Lag correlations of area-averaged, 40–80-day filtered rainfall with (a) local SST and (b) local SST tendency, using 15 years of boreal summer model output and observational data. The area is over the South China Sea (10°–15°N, 112°–117°E). Purple dashed lines represent the 95% confidence level according to the Student's t-test.

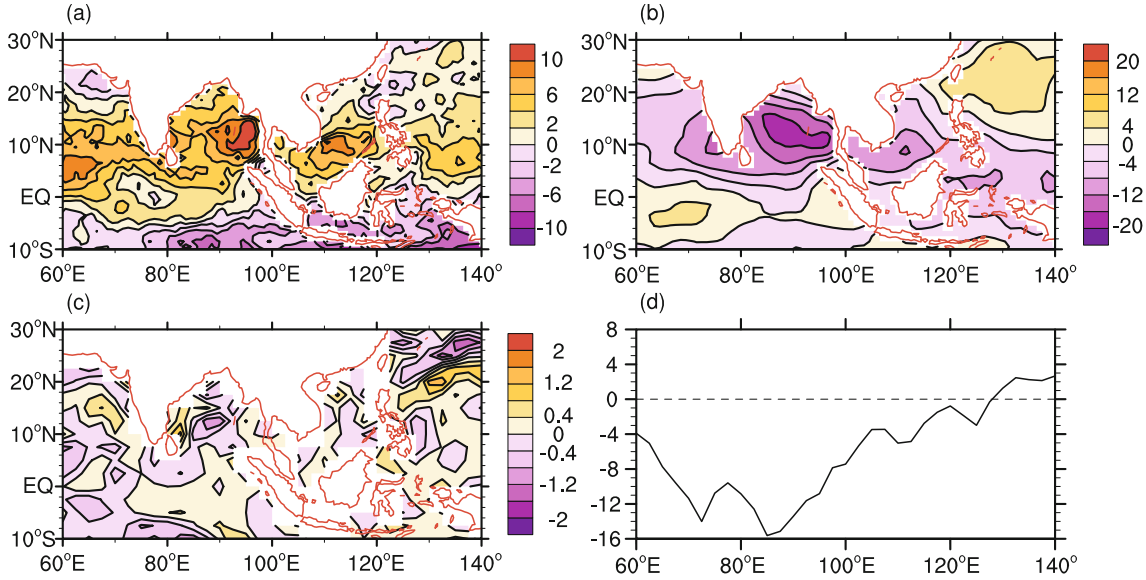

Fig. 11. The spatial distribution of anomalies of (a) net surface heat flux (positive upward; W m^{-2}); (b) net surface shortwave radiation flux (positive downward; W m^{-2}); (c) surface moisture divergence (10^6 g kg^{-1} s^{-1}); and (d) amplitudes of OLR anomalies (W m^{-2}) in Phase 7 derived from observations, with respect to latitude of convection center.

CMIP runs is that the coupled one (CMIP) takes air-sea interaction into account. The phase relationships between rainfall and SST/SST tendency simulated by CMIP are closer to the observations. The atmosphere-only model cannot realistically capture the interaction between internal physical processes and boundary conditions for ISO.

There are still some points to be confirmed and solved. Variation of air-sea interaction, on timescales from diurnal to seasonal, is believed to influence ISO simulation. Over the SAM region, it remains to be seen how air-sea interactions on various timescales work together, and which timescale is more important. Then there is the question of their influence on the internal dynamics of the atmosphere. Considering only the internal processes of the atmosphere, an aim is to

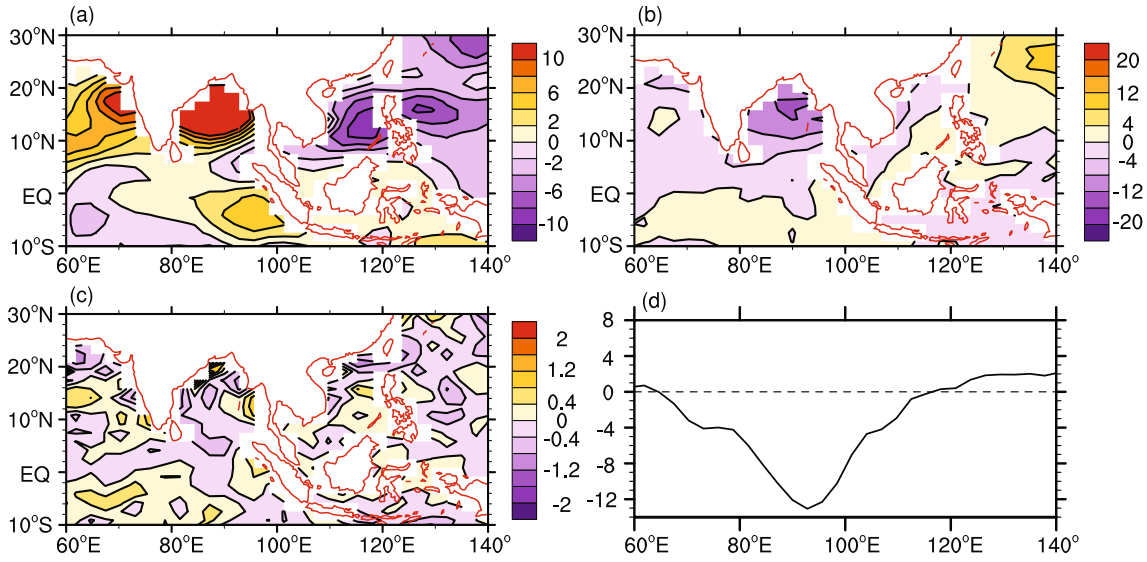

Fig. 12. The same as Fig. 11, but from AMIP data.

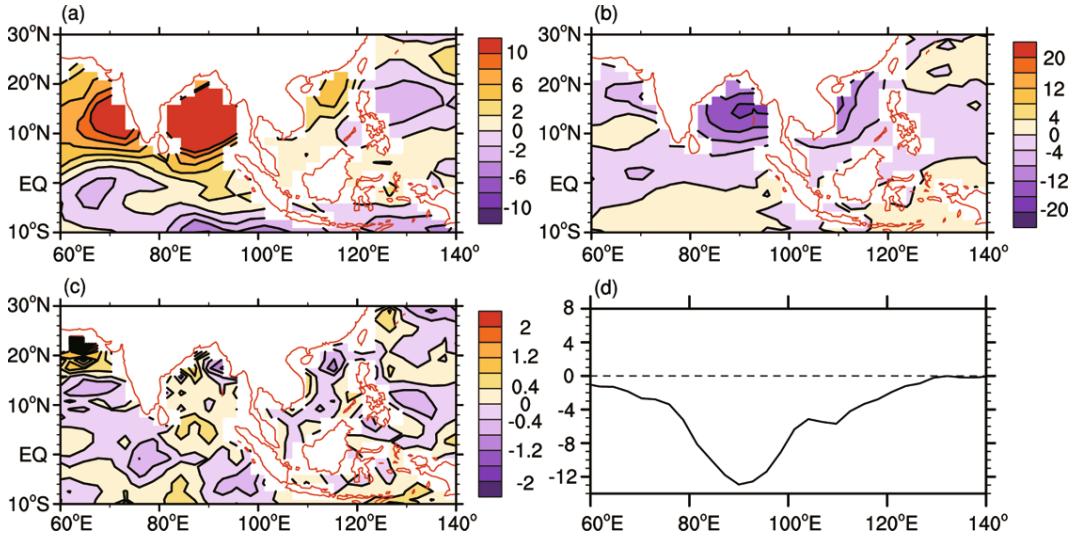

Fig. 13. The same as Fig. 11, but from CMIP data.

elucidate the factor other than air-sea interaction that drives the eastward propagation.

Regarding physical processes, aside from positive effects of air-sea interaction on the simulations, negative effects from the deficiencies in the cumulus parameterization and PBL schemes should be addressed. Cumulus parameterization is always considered the key factor in ISO simulation. Furthermore, the feedback relationship between the cumulus and PBL schemes deserves greater attention. Lin et al. (2008b) demonstrated that eastward propagation of the MJO may usually be improved with a stronger trigger of moisture convection in the PBL. Therefore, there is a need for more detailed studies of PBL physics.

Acknowledgements. The authors appreciate the constructive comments of the anonymous reviewers. This work was jointly supported by the "Strategic Priority Research Program–Climate Change: Carbon Budget and Related Issue" of the Chinese Academy of Sciences (Grant No. XDA-05110303), and the Chinese Ministry of Science and Technology (Grant Nos. 2010CB951703 and 2009CB421403).

REFERENCES

Adler, R. F., and Coauthors, 2003: The version 2 global precipitation climatology project (GPCP) Monthly Precipitation Analysis (1979–present). *Journal of Hydrometeorology*, **4**, 1147–1167.

Annamalai, H., and J. M. Slingo, 2001: Active/break cycles: Diagnosis of the intraseasonal variability of the Asian summer monsoon. *Climate Dyn.*, **18**, 85–102.

Bao, Q., G. X. Wu, Y. M. Liu, J. Yang, Z. Z. Wang, and T. J. Zhou, 2010: An introduction to the coupled model FGOALS1.1-s and Its Performance in East Asia. *Adv. Atmos. Sci.*, **27**(5), 1131–1142, doi: 10.1007/s00376-010-9177-1.

Brinkop, S., and E. Roeckner, 1995: Sensitivity of a general-circulation model to parameterizations of cloud-turbulence interactions in the atmospheric boundary-layer. *Tellus* (*A*), **47**, 197–220.

Chao, W. C., and L. Deng, 1998: Tropical intraseasonal oscillation, super cloud clusters, and cumulus convection schemes. Part II: 3D aquaplanet simulations. *J. Atmos. Sci.*, **55**, 690–709.

Edwards, J. M., and A. A. Slingo, 1996: Studies with a flexible new radiation code. I: Choosing a configuration for a large-scale model. *Quart. J. Roy. Meteor. Soc.*, **122**, 689–720.

Fu, X., and B. Wang, 2004: Differences of boreal summer intraseasonal oscillations simulated in an atmosphere-ocean coupled model and an atmosphere-only model. *J. Climate*, **17**, 1263–1271.

Fu, X., B. Wang, and T. Li, 2002: Impacts of air-sea coupling on the simulation of the mean Asian summer monsoon in the ECHAM4 model. *Mon. Wea. Rev.*, **130**, 2889–2903.

Fu, X., B. Wang, D. E. Waliser, and L. Tao, 2007: Impact of atmosphere–ocean coupling on the predictability of monsoon intraseasonal oscillations. *J. Atmos. Sci.*, **64**, 157–174.

Fu, X., B. Yang, G. Bao, and B. Wang, 2008: Sea surface temperature feedback extends the predictability of tropical intraseasonal oscillation. *Mon. Wea. Rev.*, **136**, 577–597.

Hayashi, Y., 1982: Space-time spectral analysis and its application to atmospheric waves. *J. Meteor. Soc. Japan*, **60**, 156–171.

Hendon, H. H., 2000: Impact of air-sea coupling on the Madden-Julian oscillation in a general circulation model. *J. Atmos. Sci.*, **57**, 3939–3952.

Hendon, H. H., B. Liebmann, and M. E. Newman, 2000: Mediumrange forecasts errors associated with active episodes of the Madden-Julian oscillation. *Mon. Wea. Rev.*, **128**, 69–85.

Huffman, G. J., and Coauthors, 1997: The global precipitation climatology project (GPCP) version 1 dataset. *Bull. Amer. Meteor. Soc.*, **78**, 5–20.

Inness, P. M., and J. M. Slingo, 2003: Simulation of the Madden-Julian oscillation in a coupled general circulation model. Part II: The role of the basic state. *J. Climate*, **16**, 365–382.

Jiang, X., T. Li, and B. Wang, 2004: Structures and mechanisms of the northward propagating boreal summer intraseasonal oscillation. *J. Climate*, **17**, 1022–1039.

Kang, I. S., C. H. Ho, Y. K. Lim, and K. M. Lau, 1999: Principal modes of climatological seasonal and intraseasonal variations of the Asian summer monsoon. *Mon. Wea. Rev.*, **127**, 322–340.

Kemball-Cook, S., and B. Wang, 2001: Equatorial waves and air-sea interaction in the Boreal summer intraseasonal oscillation. *J. Climate*, **14**, 2923–2942.

Kim, D., and Coauthors, 2009: Application of MJO simulation diagnostics to climate models. *J. Climate*, **22**, 6413–6436.

Lau, K. M., and P. H. Chan, 1986: Aspects of the 40–50 day oscillation during the northern summer as inferred from outgoing longwave radiation. *Mon. Wea. Rev.*, **114**, 1354–1367.

Lawrence, D. M., and P. J. Webster, 2002: The boreal summer intraseasonal oscillation: Relationship between northward and eastward movement of convection. *J. Atmos. Sci.*, **59**, 1593–1606.

Lee, M. I., I. S. Kang, B. E. Maps, and P. J. Webster, 2003: Impacts of cumulus convection parameterization on aqua-planet AGCM simulations of tropical intraseasonal variability. *J. Meteor. Soc. Japan*, **81**, 963–992.

Liebmann, B., and C. A. Smith, 1996: Description of a complete (interpolated) outgoing longwave radiation dataset. *Bull. Amer. Meteor. Soc.*, **77**, 1275–1277.

Lin, J. L., and Coauthors, 2006: Tropical intraseasonal variability in 14 IPCC AR4 climate models. Part I: Convective signals. *J. Climate*, **19**, 2665–2690.

Lin, J. L., K. M. Weickmann, G. N. Kiladis, B. E. Mapes, S. D. Schubert, M. J. Suarez, J. T. Bacmeister, and M.-I. Lee, 2008a: Subseasonal variability associated with Asian summer monsoon simulated by 14 IPCC AR4 coupled GCMs. *J. Climate*, **21**, 4541–4567.

Lin, J. L., M.-I. Lee, D.-H. Kim, I.-S. Kang, and D. Frierson, 2008b: The impacts of convective parameterization and moisture triggerring on AGCM-simulated convectively coupled equatorial waves. *J. Climate*, **21**, 883–909.

Liu, H. L., X. Zhang, W. Li, Y. Yu, and R. Yu, 2004: An eddy-permitting oceanic general circulation model and its preliminary evaluations. *Adv. Atmos. Sci.*, **21**, 675–690.

Liu, P., B. Wang, K. Sperber, and J. Meehl, 2005: MJO in the NCAR CAM2 with the Tiedtke convection scheme. *J. Climate*, **18**, 3007–3020.

Liu, Y. M., Q. Bao, A. M. Duan, Z. A. Qian, and G. X. Wu, 2007: Recent progress in the impact of the Tibetan Plateau on climate in China. *Adv. Atmos. Sci.*, **24**, 1060–1076, doi: 10.1007/s00376-007-1060-3.

Mao, J. Y., and J. C. L. Chan, 2005: Intraseasonal variability of the South China Sea summer monsoon. *J. Climate.*, **18**, 2388–2402.

Nakazawa, T., 1992: Seasonal phase lock of intraseasonal variation during the Asian summer monsoon. *J. Meteor. Soc. Japan.*, **70**, 257–273.

Nordeng, T. E., 1994: Extended versions of the convective parameterization scheme at ECMWF and their impact on the mean and transient activity of the model in the tropics. ECMWF Tech. Memo., **206**, Reading, England, 41pp.

Reynolds, R. W., N. A. Rayner, T. M. Smith, D. C. Stokes, and W. Wang, 2002: An improved in situ and satellite SST analysis for climate. *J. Climate*,

15, 1609–1625.

Schiffer, R. A., and W. B. Rossow, 1985: ISCCP global radiance data set: A new resource for climate research. *Bull. Amer. Meteor. Soc.*, **66**, 1498–1505.

Seo, K. H., and W. Wang, 2010: The Madden–Julian oscillation simulated in the NCEP climate forecast system model: The importance of stratiform Heating. *J Climate*, **23**, 4770–4793.

Song, X. L., 2005: The evaluation analysis of two kinds of mass flux cumulus parameterizations in climate simulation, Ph. D. dissertation, Institute of Atmospheric Physics, Chinese Academy of Sciences, 119–145. (in Chinese)

Sun, Z., and L. Rikus, 1999a: Improved application of ESFT to inhomogeneous atmosphere. *J. Geophys. Res.*, **104**, 6291–6303.

Sun, Z., and L. Rikus, 1999b: Parameterization of effective radius of cirrus clouds and its verification against observations. *Quart. J. Roy. Meteor. Soc.*, **125**, 3037–3056.

Taylor, K. E., R. J. Stouffer, and G. A. Meehl, 2009: A summary of the CMIP5 experiment design. [Available online at http://cmip-pcmdi.llnl.gov/cmip5/docs/Taylor_CMIP5_design.pdf.]

Teng, H. Y., and B. Wang, 2003: Interannual variations of the boreal summer intraseasonal oscillation in the Asian-Pacific region. *J. Climate*, **16**, 3572–3584.

Waliser, D. E., K. E. Lau, and J. H. Kim, 1999: The influence of coupled sea surface temperatures on the Madden-Julian oscillation: A model perturbation experiment. *J. Atmos. Sci.*, **56**, 333–358.

Waliser, D. E., and Coauthors, 2003: AGCM simulations of intraseasonal variability associated with the Asian summer monsoon. *Climate Dyn.*, **21**, 423–446.

Wang, B., 2005: Theories. *Intraseasonal Variability of the Atmosphere-ocean Climate System*, K. M. Lau and D. E. Waliser, Eds., Springer-Verlag, Heidelberg, Germany, 436pp.

Wang, B., and X. H. Xu, 1997: Northern Hemisphere summer monsoon singularities and climatological intraseasonal oscillation. *J. Climate*, **10**, 1071–1085.

Wheeler, M., and G. N. Kiladis, 1999: Convectively coupled equatorial waves: Analysis of clouds and temperature in the wavenumber-frequency domain. *J. Atmos. Sci.*, **56**, 374–399.

Wu, G. X., and Y. S. Zhang, 1998: Tibetan Plateau forcing and the timing of the monsoon onset over South Asia and the South China Sea. *Mon. Wea. Rev.*, **126**, 913–927.

Wu, R., and J. L. Kinter, 2010: Atmosphere-ocean relationship in the midlatitude North Pacific: Seasonal dependence and East-West Contrast. *J. Geophys. Res.*, **115**, D06101, doi: 10.1029/2009JD012579.

Yang, J., B. Wang, B. Wang, and L. J. Li, 2009: The East Asia-western North Pacific boreal summer intraseasonal oscillation simulated in GAMIL 1.1.1. *Adv. Atmos. Sci.*, **26**(3), 480–492, doi: 10.1007/s00376-009-0480-7.

Yasunari, T., 1979: Cloudiness fluctuations associated with the Northern Hemisphere summer monsoon. *J. Meteor. Soc. Japan.*, **57**, 227–242.

Yasunari, T., 1980: A quasi-stationary appearance of the 30–40 day period in the cloudiness fluctuations during the summer monsoon over India. *J. Meteor. Soc. Japan.*, **59**, 336–354.

Yu, L., X. Jin, and R. A. Weller, 2008: Multidecade global flux datasets from the objectively analyzed air-sea fluxes (OAFlux) project: Latent and sensible heat fluxes, ocean evaporation, and related surface meteorological variables. OAFlux Project Tech. Rep. OA-2008-01, Woods Hole Oceanographic Institution, Woods Hole, Massachusetts, 64pp.

Zhang, C., and Coauthors, 2006: Simulations of the Madden-Julian oscillation in four pairs of coupled and uncoupled global models. *Climate Dyn.*, **27**, 573–592.